Effects of Formate Binding to a Bipyridine-Based

Cobalt-4N Complex

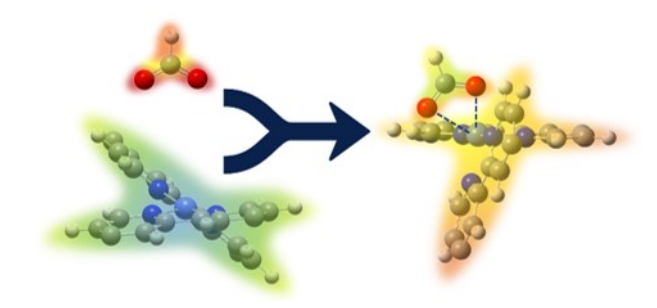
Madison M. Foreman, Rebecca J. Hirsch, J. Mathias Weber*

JILA and Department of Chemistry, University of Colorado Boulder, 440 UCB, Boulder, CO 80309-0440, USA

Abstract

We report the vibrational spectrum of a metal organic complex consisting of a Co center surrounded by two bipyridine-based ligands, and explore the change of the spectrum upon addition of a formate ligand to the complex. We assign the spectra using density functional theory. The spectra encode the binding motif of the formate to the metal, and the calculated charge distributions highlight the ability of the organic ligand framework to act as charge reservoirs modulating the redox properties of the metal center.

TOC Figure



Introduction

In many organometallic catalysts, transition metal centers are surrounded by organic ligands that coordinate to the metal center through four nitrogen atoms (M-4N complexes), such as porphyrins, 1-3 phthalocyanines, 2 cyclam, 4-5 and polypyridines. 6-9 The organic ligands govern the accessibility of the metal center by solvent molecules or substrates through steric effects and by occupying four metal coordination sites, and they can act as charge reservoirs, modifying the redox properties of the metal center. At the same time, the electronic properties of the metal center influence the orientation of the ligands to each other, and the resulting structure and charge distribution in the complex is the product of the interplay between metal center and ligands.

In catalysis applications of M-4N complexes, the open coordination positions of the metal center are occupied by a changing set of ligands over the course of the catalytic cycle — from its resting state through complexes with the substrate, reaction intermediates, and then to the product. This changing ligand shell results in concomitant changes to the geometry and charge distribution of the rest of the molecule, including the 4N ligands. The molecular details of these changes are difficult to study in the condensed phase, particularly in reactive solutions or under turnover conditions encountered in catalysis, due to the interaction with the chemical environment and the large number of different species present in such circumstances. An alternative route to the detailed characterization of relevant molecules is to use mass spectrometric preparation of ionic complexes by electrospray ionization (ESI) in tandem with laser spectroscopy, 10-17 circumventing many of the complications of speciation in solutions.

In the present work, we use complexes where a cobalt center is surrounded by two DTBbpy ligands (DTBbpy = 4,4'-di(*tert*-butyl)-2,2'-bipyridine), forming a dication, [Co(DTBbpy)₂]²⁺ (compound $\mathbf{1}^{2+}$ in Scheme 1). We use infrared photodissociation spectroscopy enabled by N₂

messenger tagging to investigate changes in the properties of 1^{2+} upon coordination with formate ions, resulting in the monocationic complex [HCOO⁻·Co(DTBbpy)₂]⁺ (compound 2^+ in Scheme 1). While we do not follow a complete catalytic cycle, these complexes can be thought of as model systems in the context of CO₂ reduction catalysis, where formate is one of the possible products observed. We compare our experimental results with predicted infrared spectra based on density functional theory (DFT) calculations.

Scheme 1. Representations of compounds 1^{2+} (left) and 2^{+} (right), with R = tert-butyl.

Methods

We prepared solutions containing 1^{2^+} by dissolving ca. 5 µmol of Co(NO₃)₂·6H₂O (Sigma-Aldrich, \geq 98%) and 10 µmol of DTBbpy (Sigma-Aldrich, 98%) in 5.75 mL methanol (Macron, \geq 99.8%). Adding formate to these solutions at ca. 100-fold excess resulted in preparation of compound 2^+ . Formate was produced by titrating formic acid (Sigma-Aldrich, \geq 95%) with aqueous KOH (Fisher-Scientific) until a pH of 8-9 was achieved to ensure the formic acid was completely converted to formate anions. All chemicals were used as purchased, and all solutions were sprayed without further purification.

The experimental setup has been described in detail in previous work,²¹ and only a brief description will be given here. Upon electrospray ionization from solutions prepared as described above, ions pass through a stainless steel desolvation capillary and a skimmer, entering a sequence of octopole ion guides. The ion guides and subsequent ion optics transfer the ions through several differential pumping stages into a Paul trap mounted on a closed cycle He cryostat, and held at 20 – 30 K. In the Paul trap, ions are cooled in collisions with D₂ buffer gas and tagged with N₂ molecules. We note that attempts to attach CO₂ to compound 1²⁺ by adding CO₂ in the cryogenic

trap or the octopole region, or by using a CO₂ saturated solution for electrospray, were unsuccessful.

After ca. 100 ms cooling time (10 Hz repetition rate of the trap and mass spectrometer), ions are ejected from the trap into the acceleration region of a time-of-flight mass spectrometer. The target ions for a given experiment are mass-selected using a pulsed mass gate, and the mass-selected ions are irradiated with the output of a tunable infrared optical parametric converter system (bandwidth ca. 2 cm⁻¹, pulse duration 5-7 ns). If infrared photons are absorbed, redistribution of the vibrational excitation energy in the target complexes results in the loss of N₂ messenger tags by vibrational predissociation. The resulting photofragments are separated from the undissociated parent ions using a two-stage reflectron as a second mass spectrometry step. The intensity of fragment ions is monitored as a function of the infrared wavenumber, and divided by the infrared photon number per pulse, which is also monitored. The laser is fired every second experimental cycle of the mass spectrometer to subtract background signals from unimolecular or collision-induced decay of target ions. In each spectrum, 16 laser shots were averaged for each data point, and for each target ion species, several spectra were measured on different days and averaged to ensure reproducibility and improve the signal-to-noise ratio.

Geometry optimizations and vibrational spectra of all complexes under study were performed using spin-unrestricted DFT (B3LYP functional,²² cc-pVDZ basis sets²³ for all atoms). All geometries shown in this work are minimum energy structures, and all complexes have doublet spin states. Partial charges in the complexes were calculated for these minimum energy structures based on natural population analysis.²⁴ The infrared spectra of all complexes were calculated using the harmonic approximation. All calculations were performed using Gaussian 16.²⁵

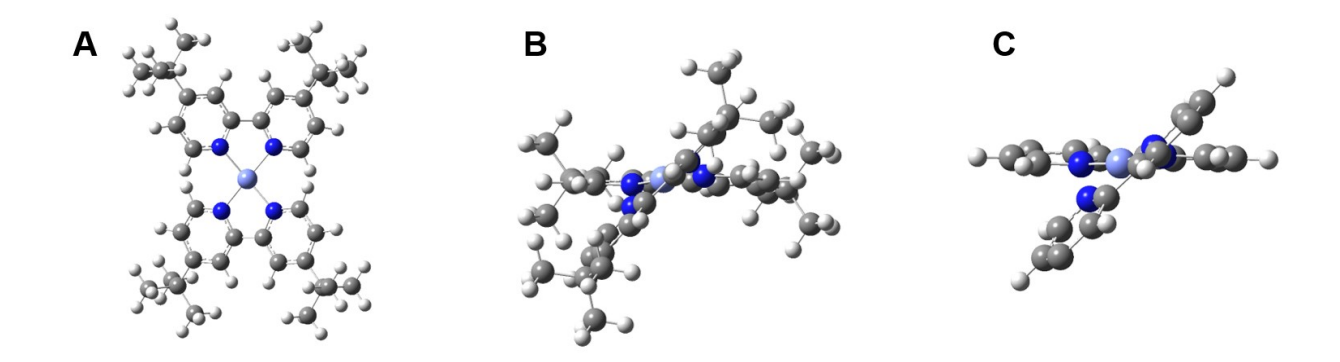


Figure 1. Different views of compound 1^{2+} . A: C₂ symmetry axis (approximate, see text) perpendicular to the plane of drawing; B: bipyridine planes of the DTBbpy ligands perpendicular to the plane of drawing; C: a similar view as in part B, but with the *tert*-butyl ligands removed to show only the bipyridine parts of the ligands. Atom colors: C = gray; $C = \text{gray$

Results and Discussion

The calculated structure of 1^{2+} is shown in Figure 1. The complex has approximately C_2 structure, with a coordination motif roughly between square planar and tetrahedral. The DTBbpy ligands are slightly buckled, and the NN-NN dihedral angle between the ligands is 138.5°. The Co metal center is slightly closer to one of the N atoms on each ligand, with distances of 197 pm and 198 pm, respectively.

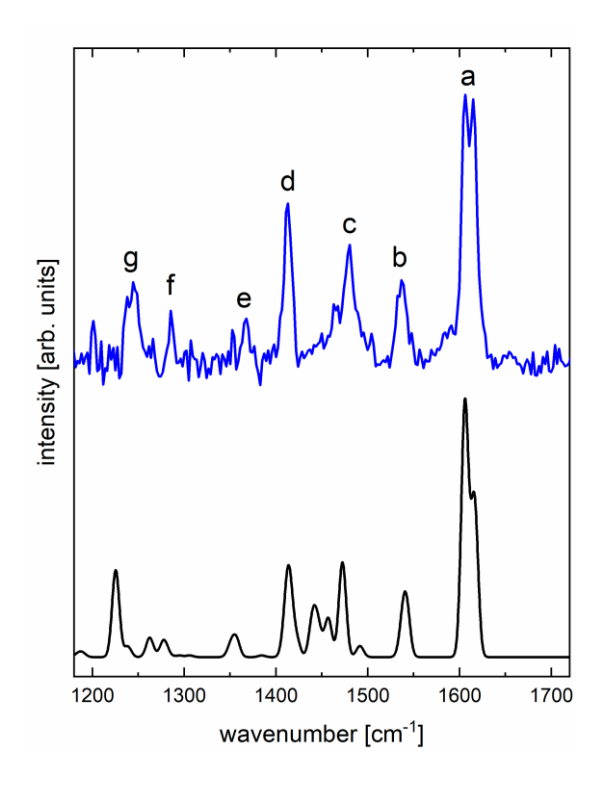


Figure 2. Comparison of experimental (top trace) and simulated (bottom trace) spectrum of 1^{2+} . The frequencies in the simulated spectrum were scaled by 0.975 for optimal match with the experiment. The calculated frequencies were used to create the simulated spectrum by superimposing Gaussian lines with 9 cm⁻¹ FWHM, corresponding to the width of the narrowest features observed in the experimental spectrum. See text for discussion of labeled features.

Figure 2 shows the experimental spectrum of 1^{2+} in the fingerprint region compared to the predicted infrared spectrum. The spectrum consists of several sharp transitions above 1000 cm⁻¹, with particularly prominent features between 1400 cm⁻¹ and 1650 cm⁻¹. Two structures were optimized that include the N_2 messenger tag, contrasting the case of binding to the metal center vs. attached to one of the *tert*-butyl groups on one of the ligands (see Supporting Information). While their calculated energies show that the structure with N_2 binding to the metal center is 100 meV lower in energy, the resulting simulated infrared spectra are insensitive to the N_2 messenger tag position; their calculated frequencies differ by < 2 cm⁻¹. We will therefore ignore the N_2 tag position in our analysis of the vibrational spectrum of 1^{2+} .

Scaling the harmonic frequencies of the simulated infrared spectrum by 0.975, we obtain an excellent match between the experimental and simulated infrared spectrum, allowing us to assign the most prominent peaks. Generally, the features above 1475 cm⁻¹ can be assigned to modes largely localized on the bipyridine moieties, while the lower frequency features also involve the tert-butyl residues. The highest frequency feature (a) is a doublet with peaks at 1606 cm⁻¹ and 1615 cm⁻¹, respectively. The two components can be assigned to modes in the bipyridine rings of the ligands that combine C-C stretching and in-ring-plane CH wagging motions, where the motions of each bipyridine ring are coupled in phase in the lower frequency peak and out of phase in the higher frequency peak (see Supporting Information for selected vibrational patterns). Feature (b) at 1536 cm⁻¹ mainly consists of two unresolved peaks corresponding to antisymmetric C-N-C stretching (and concomitant CH wagging) modes, again localized on the bipyridine rings, with similar phase relations as those resolved in the highest frequency doublet. A broad feature at 1479 cm⁻¹ (c) envelops several unresolved transitions, where the most intense peak is calculated to contain the signatures of symmetric C-N-C stretching modes on the bipyridine rings. On its high frequency side, the calculations predict the signature of the C-C stretching motion of the bond connecting the rings in each DTBbpy ligand, coupled to a symmetric C-N-C stretching motion. Its lower energy side contains unresolved HCH bending modes in the tert-butyl groups. We assign the sharp peak at 1413 cm⁻¹ (d) to a group of bipyridine ring deformation modes that also involve HCH bending motions on the tert-butyl groups. The weak feature at 1367 cm⁻¹ (e) is the combined signature of several modes with methyl group umbrella motions. A similarly weak peak at 1286 cm⁻¹ (f) is consistent with a ring deformation mode or with an in-plane CH wagging mode. Since both are predicted to be in this region, we refrain at this point from a more definitive assignment. Finally, peak (g) at 1245 cm⁻¹ can be assigned to a mode that is mainly characterized by C(CH₃)₃

umbrella motion on the *tert*-butyl residues. The mode assignment is summarized in Supporting Information.

Upon addition of formate to the metal center, the complex undergoes structural changes that are encoded in the infrared spectrum. Figure 3 shows a comparison of the infrared spectrum of $\mathbf{1}^{2+}$ with that of the formate complex, $\mathbf{2}^{+}$. Several additional features appear, which belong to vibrational modes of the formate ligand. Moreover, we observe a general red shift (by $< 20 \text{ cm}^{-1}$) of the peaks identified above as belonging to the DTBbpy ligands.

Before assigning features to vibrational modes, it is important to characterize the geometry of the complex, since we found several minimum energy structures as shown in Figure 4. The lowest energy structure (A) shows the formate ligand bound in an asymmetric bidentate arrangement to the metal center where the distances between the O atoms and the metal center are 198 pm and 241 pm, respectively. In a similar structure (B) 314 meV higher in energy, the formate ligand attaches with only one of the two O atoms (191 pm Co-O distance), with the other much further away from the metal center (324 pm). Finally, we also found an isomer where the ligand binds with the C atom to the metal center (C). This isomer is ca. 1 eV higher in energy than isomer A, and while the composition of the ligand is [H, C, 2O], it adopts the structure of a carboxylic acid group, R-COOH, with R being the metal center.

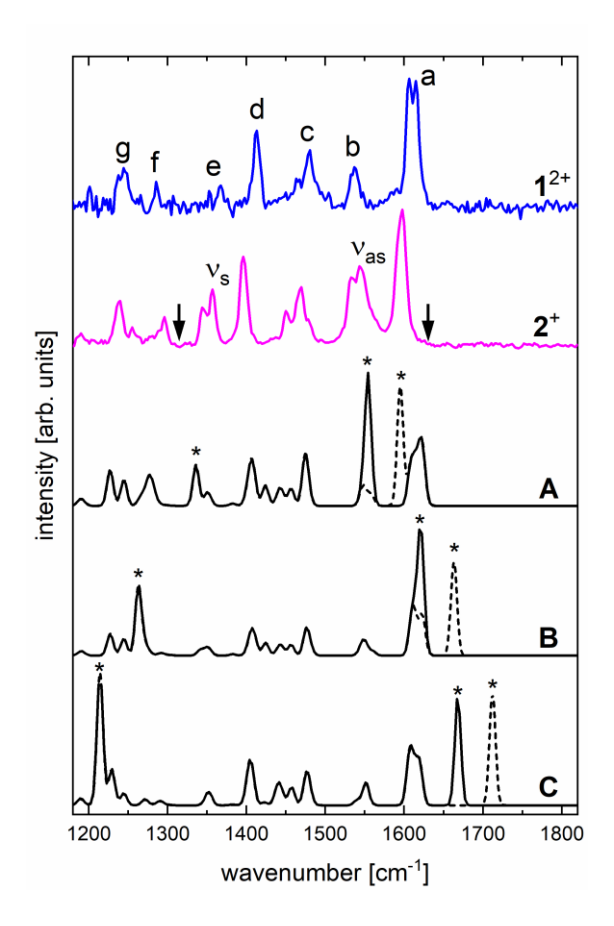


Figure 3. The top two traces show experimental spectra of 1^{2+} and 2^+ . The bottom three traces are simulated spectra of different calculated isomers of 2^+ , with labels as in Figure 4. All modes except the antisymmetric stretching mode of the formate moiety (v_{as}) were generally scaled by 0.975. The dashed lines in the calculated spectra correspond to a scaling factor 0.975 for v_{as} , while the full lines scale this mode by 0.95 (see text). The positions of the OCO stretching modes of the formate ligand are marked with asterisks, while the arrows mark the analogous modes for free formate. The calculated frequencies were used to create the simulated spectrum by superimposing Gaussian lines with 9 cm⁻¹ FWHM, corresponding to the width of the narrowest features observed in the experimental spectrum.

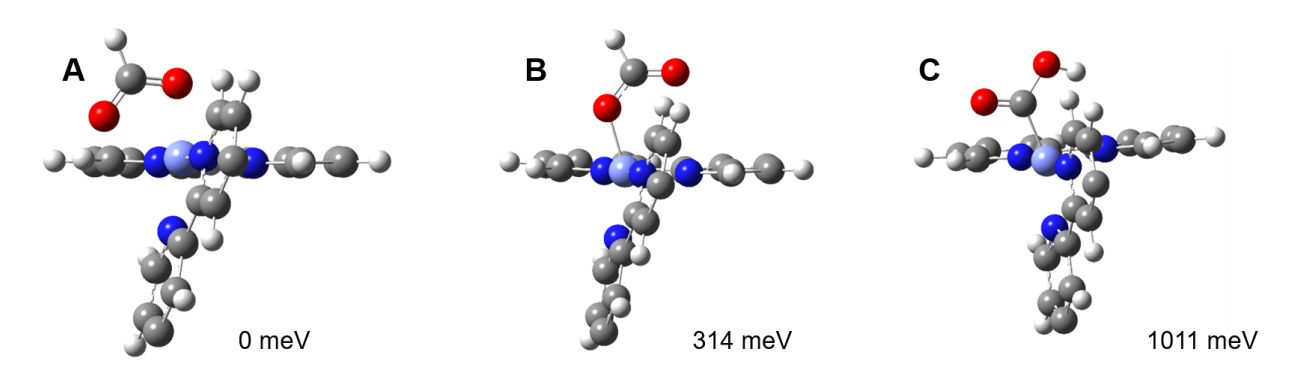


Figure 4. Calculated isomers of compound 2^+ , with the *tert*-butyl ligands removed to show only the bipyridine parts of the ligands for clarity. A: bidentate formate-metal interaction; B: monodentate formate-metal interaction; C: formyl-metal interaction via a Co-C bond. Atom colors: C = gray; H = white; N = dark blue; C = light blue; C = red.

To identify the isomer relevant for the infrared spectrum of 2⁺, it is useful to identify the main differences between the infrared spectra of 1²⁺ and 2⁺, which should be due to the appearance of formate modes, particularly OCO stretching vibrations. In spectrum of 2⁺, feature (a) collapses into a single peak, while feature (b) splits into two peaks and increases in relative intensity compared to feature (a) by about a factor of 2. In addition, a new intense signature appears in the region of feature (e). We use the appearance of new, intense features to locate the two OCO stretching vibrations of the formate ligand, assigning the more intense of the components in the region of feature (b) at 1545 cm⁻¹ to the antisymmetric OCO stretching mode (v_{as}) of the formate ligand, shifted by ca. -80 cm⁻¹ from the value of free formate.²⁶ The more intense component in the region of feature (e) at 1357 cm⁻¹ is the signature of the symmetric OCO stretching mode (ν_s), blue-shifted from the position in free formate by 43 cm⁻¹. The identification of the two OCO stretching modes in the experimental spectrum allows us to identify the structure of the complex. Using the same scaling factor as for complex 1^{2+} (0.975), the calculated spectra in Figure 3 show the OCO stretching vibrations marked with asterisks on the dashed lines. The splitting between the two vibrational modes v_s and v_{as} is strongly dependent on the interaction of the formate ligand and the metal center. Isomer A is clearly the calculated structure where this splitting is most compatible with that observed in the experimental spectrum of the formate complex 2⁺. The signature of the in-plane OCH bending vibration of the formate ligand for this structure appears in the region of feature (f), at 1296 cm⁻¹, and is calculated to be the strongest transition of this feature. The mode assignment is summarized in Supporting Information.

While the calculated positions of v_3 and v_{as} for isomer A are only qualitatively consistent with the experimental spectrum, the modes of the DTBbpy ligands are nearly quantitatively recovered. Based on this observation, the calculated frequencies of the OCO stretching vibrations and their scaling deserve additional attention. In principle, there is no reason to expect that all vibrational modes of a molecule should have the same scaling factor, as their anharmonicities depend on the nature of the bonds involved in the vibrational mode patterns. From this point of view, the close match of the simulation with a single scaling factor for all modes to the experimental spectrum of compound 1^{2+} is likely to be fortuitous. The same scaling factor does not seem to work as well for the OCO vibrations of the formate ligand in 2^+ , particularly v_{as} . Comparison of v_{as} in the experimental spectrum of formate 26 with the calculated spectrum of this ion at the same level of theory used here could be expected to yield a reasonable scaling factor. However, this calculation (scaling factor 0.917) would place v_{as} at 1500 cm $^{-1}$, just above feature (c), which results in a deviation from the experimental value similar in magnitude to treating all modes with the same scaling factor.

The difficulty of obtaining a good match between experiment and computation for these modes can be traced to the role of negative charge in and the geometry of the formate ligand. The positions of the symmetric (ν_s) and antisymmetric (ν_{as}) stretching frequencies in species of the form R-COO are governed by two contributions.²⁷ The first is the mechanical coupling of the two CO oscillators, determined through the OCO bond angle, and the second is the bond strength of the CO bonds. Both of these contributions are quite sensitive to the charge in the (net antibonding) HOMO of the carboxylate group, which in turn is affected by the proximity of the metal center in the present case. Increasing the negative charge on the carboxylate makes the OCO bond angle more acute and thereby reduces the splitting between ν_s and ν_{as} , shifting ν_{as} to the red and ν_s to the blue. In

contrast, the weakening of the CO bonds upon increasing the charge on the carboxylate shifts both modes to the red. Both effects shift v_{as} in the same direction, while they partially cancel each other for v_s . At the same time, the proximity of the formate ligand to the metal center will have a strong effect on both the charge distribution and the force constants of the CO bonds in the formate ligand through Coulomb interaction between the metal and the O atoms, similar to other R–COO groups in the vicinity of a divalent metal.²⁸ The sensitivity of the OCO stretching vibrations to the combination of these effects makes accurate computational treatments rather challenging. Here, we can infer the dominating effects by comparing the OCO stretching modes, geometries and charge distributions of free formate and the formate ligand in 2⁺. Judging from the calculated charges on the COO group alone, we would expect the larger negative charge on free formate (-0.948 e) to lead to a more acute OCO bond angle than in the formate ligand in 2^+ (-0.659 e). However, this should lead to a smaller splitting of v_{as} and v_{s} in free formate, together with a lower value of v_{as} in free formate. The experimental values²⁶ behave opposite to this expectation (see Figure 3), and they are consistent with the calculated OCO bond angles (131° for free formate, 122° for the formate ligand in 2⁺). Since this behavior cannot be explained with the charge distribution in the formate ligand, we infer that the Coulomb interaction with the metal ion in the bidentate binding motif forces the OCO bond angle in the formate ligand to smaller values. The more acute bond angle results in decoupling the two CO oscillators beyond what we would have expected based on the charge distribution alone, leading to the splitting we observe experimentally.

Table 1. Calculated Charge Distributions (a)

Complex	1 ^{2+ (b)}	2^{+}	

Co	0.746 (0.857)	0.600
DTBbpy ligands	1.147 (1.139)	0.917
Small ligand (c)	0.107 (0.004)	-0.517

- (a) See Supporting Information for more details.
- (b) Numbers in parentheses are results for the isomer with the N₂ messenger tag binding to a DTBbpy ligand.
- (c) N₂ or formate.

The overall charge distribution in the complexes studied here is summarized in Table 1. This is of interest in the context of metal-4N complexes as the ligand environment is key in tuning the effective oxidation state of the metal. Co(II) salts were used to prepare both 1^{2+} and 2^+ , and one could naively assume that the Co atom would be formally characterized as Co^{2+} . The size of both complexes under study necessitates the use of DFT and relatively small basis sets, so the results of any population analysis should be taken as qualitative in nature. Nonetheless, it is interesting to note that natural population analysis shows that the cobalt atom carries less than +1 e charge in both complexes (Mulliken analysis gives qualitatively similar results). For 1^{2+} , the N_2 ligand only plays a minor role (as expected), and the rest of the +2 e charge of the complex resides in the DTBbpy framework. For the formate complex 2^+ , the population analysis predicts substantial charge transfer from the formate ligand to the rest of the complex (ca. 0.5 e), which is accommodated by the metal center and the DTBbpy ligands. These charge distributions show the ability of the organic ligand framework in metal-4N compounds to act as charge reservoirs playing a powerful role in governing the redox properties of these complexes.

Conclusions

We used N₂ messenger tagging to measure the vibrational spectra of a bipyridine-based Co complex with and without a formate ligand in the fingerprint region. We found by computational analysis of the vibrational spectrum of [Co(DTBbpy)₂]²⁺ (compound 1²⁺) that the spectrum is not sensitive to the position of the N₂ tag, even if it binds directly to the metal center. The vibrational modes of DTBbpy ligands are well recovered by scaled harmonic DFT calculations. They show small red shifts upon addition of a formate ligand, which are likely due to additional negative charge accommodated by the DTBbpy ligands. The formate ligand binds in an asymmetric bidentate fashion to the metal center, which is clearly established by the positions of the symmetric and antisymmetric OCO stretching vibrations of the formate moiety. These modes appear as new, intense features in the vibrational spectrum of the complex [HCOO⁻·Co(DTBbpy)₂]⁺, compound 2⁺. The calculated charge distributions in the two complexes show that the Co metal center carries less than a single positive charge, highlighting the ability of the organic network to accommodate charge.

ASSOCIATED CONTENT

Supporting Information. The following files are available free of charge: Structures and vibrational spectra for compounds 1²⁺ and 2⁺; illustration of vibrational patterns of motion of selected DTBbpy vibrations; population analysis; assignments of prominent infrared features.

AUTHOR INFORMATION

Corresponding Author

*J. Mathias Weber – JILA and Department of Chemistry, University of Colorado, Boulder, Colorado 80309-0440, United States; orcid.org/0000-0002-5493-5886; Phone: +1-303-492-7841; Email: weberjm@jila.colorado.edu

Authors

Madison M. Foreman – JILA and Department of Chemistry, University of Colorado, Boulder, Colorado 80309-0440, United States

Rebecca J. Hirsch – JILA and Department of Chemistry, University of Colorado, Boulder, Colorado 80309-0440, United States

Notes

The authors declare no competing financial interest.

ACKNOWLEDGMENT

We gratefully acknowledge support from the U. S. National Science Foundation under award no. CHE-1764191. This work utilized resources from the University of Colorado Boulder Research

Computing Group, which is supported by the National Science Foundation (awards ACI-1532235 and ACI-1532236), the University of Colorado Boulder, and Colorado State University.

REFERENCES

- (1) Saveant, J.-M. Molecular Catalysis of Electrochemical Reactions. Mechanistic Aspects. *Chem. Rev.* **2008**, *108*, 2348-2378.
- (2) Manbeck, G. F.; Fujita, E. A Review of Iron and Cobalt Porphyrins, Phthalocyanines and Related Complexes for Electrochemical and Photochemical Reduction of Carbon Dioxide. *J. Porphyr. Phthalocyanines* **2015**, *19*, 45-64.
- (3) Lin, S.; Diercks, C. S.; Zhang, Y.-B.; Kornienko, N.; Nichols, E. M.; Zhao, Y.; Paris, A. R.; Kim, D.; Yang, P.; Yaghi, O. M. et al. Covalent Organic Frameworks Comprising Cobalt Porphyrins for Catalytic CO₂ Reduction in Water. *Science* **2015**, *349*, 1208-1213.
- (4) Beley, M.; Collin, J. P.; Ruppert, R.; Sauvage, J. P. Electrocatalytic Reduction of CO₂ by Ni Cyclam²⁺ in Water: Study of the Factors Affecting the Efficiency and the Selectivity of the Process. *J. Am. Chem. Soc.* **1986**, *108*, 7461-7467.
- (5) Ogata, T.; Yanagida, S.; Brunschwig, B. S.; Fujita, E. Mechanistic and Kinetic Studies of Cobalt Macrocycles in a Photochemical CO₂ Reduction System Evidence of Co-CO₂ Adducts as Intermediates. *J. Am. Chem. Soc.* **1995**, *117*, 6708-6716.
- (6) Hawecker, J.; Lehn, J. M.; Ziessel, R. Electrocatalytic Reduction of Carbon Dioxide Mediated by Re(Bipy)(CO)₃Cl (Bipy = 2,2'-Bipyridine). *J. Chem. Soc., Chem. Comm.* **1984**, 328-330.
- (7) Keith, J. A.; Grice, K. A.; Kubiak, C. P.; Carter, E. A. Elucidation of the Selectivity of Proton-Dependent Electrocatalytic CO₂ Reduction by *fac*-Re(Bpy)(CO)₃Cl. *J. Am. Chem. Soc.* **2013**, *135*, 15823-15829.

- (8) Takeda, H.; Koizumi, H.; Okamoto, K.; Ishitani, O. Photocatalytic CO₂ Reduction Using a Mn Complex as a Catalyst. *Chem. Commun.* **2014**, *50*, 1491-1493.
- (9) Tanaka, K.; Ooyama, D. Multi-Electron Reduction of CO₂ Via Ru-CO₂, -C(O)OH, -CO, -CHO, and -CH₂OH Species. *Coordin. Chem. Rev.* **2002**, *226*, 211-218.
- (10) Craig, S. M.; Menges, F. S.; Johnson, M. A. Application of Gas Phase Cryogenic Vibrational Spectroscopy to Characterize the CO₂, CO, N₂ and N₂O Interactions with the Open Coordination Site on a Ni(I) Macrocycle Using Dual Cryogenic Ion Traps. *J. Mol. Spectrosc.* **2017**, *332*, 117-123.
- (11) Duffy, E. M.; Marsh, B. M.; Voss, J. M.; Garand, E. Characterization of the Oxygen Binding Motif in a Ruthenium Water Oxidation Catalyst by Vibrational Spectroscopy. *Angew. Chem. Int. Ed.* **2016**, *55*, 4079-4082.
- (12) Garand, E.; Fournier, J. A.; Kamrath, M. Z.; Schley, N. D.; Crabtree, R. H.; Johnson, M. A. Characterization of an Activated Iridium Water Splitting Catalyst Using Infrared Photodissociation of H₂ Tagged Ions. *Phys. Chem. Chem. Phys.* **2012**, *14*, 10109-10113.
- (13) Xu, S.; Smith, J. E. T.; Gozem, S.; Krylov, A. I.; Weber, J. M. Electronic Spectra of Tris(2,2'-Bipyridine)-M(II) Complex Ions in Vacuo (M = Fe and Os). *Inorg. Chem.* **2017**, *56*, 7029-7037.
- (14) Xu, S.; Smith, J. E. T.; Weber, J. M. Ligand Influence on the Electronic Spectra of Dicationic Ruthenium-Bipyridine-Terpyridine Complexes. *J. Phys. Chem. A* **2016**, *120* 2350–2356.

- (15) Xu, S.; Smith, J. E. T.; Weber, J. M. Hydration of a Binding Site with Restricted Solvent Access Solvatochromic Shift of the Electronic Spectrum of a Ruthenium Polypyridine Complex, One Molecule at a Time. *J. Phys. Chem. A* **2016**, *120*, 7650–7658.
- (16) Xu, S.; Smith, J. E. T.; Weber, J. M. The Electronic Spectrum of Cryogenic Ruthenium-Tris-Bipyridine Dications in Vacuo. *J. Chem. Phys.* **2016**, *145*, 024304.
- (17) Xu, S.; Weber, J. M. Absorption Spectrum of a Ru(II)-Aquo Complex in Vacuo: Resolving Individual Charge-Transfer Transitions. *J. Phys. Chem. A* **2015**, *119*, 11509-11513.
- (18) Shimoda, T.; Morishima, T.; Kodama, K.; Hirose, T.; Polyansky, D. E.; Manbeck, G. F.; Muckerman, J. T.; Fujita, E. Photocatalytic CO₂ Reduction by Trigonal-Bipyramidal Cobalt(II) Polypyridyl Complexes: The Nature of Cobalt(I) and Cobalt(0) Complexes Upon Their Reactions with CO₂, CO, or Proton. *Inorg. Chem.* **2018**, *57*, 5486-5498.
- (19) Bochlin, Y.; Korin, E.; Bettelheim, A. Different Pathways for CO₂ Electrocatalytic Reduction by Confined CoTMPyP in Electrodeposited Reduced Graphene Oxide. *ACS Appl. Energy Mater.* **2019**, *2*, 8434-8440.
- (20) Dey, S.; Todorova, T. K.; Fontecave, M.; Mougel, V. Electroreduction of CO₂ to Formate with Low Overpotential Using Cobalt Pyridine Thiolate Complexes. *Angew. Chem. Int. Ed.* **2020**, *59*, 15726-15733.
- (21) Xu, S.; Gozem, S.; Krylov, A. I.; Christopher, C. R.; Mathias Weber, J. Ligand Influence on the Electronic Spectra of Monocationic Copper-Bipyridine Complexes. *Phys. Chem. Chem. Phys.* **2015**, *17*, 31938-31946.

- (22) Becke, A. D. Density-Functional Thermochemistry .3. The Role of Exact Exchange. *J. Chem. Phys.* **1993**, *98*, 5648-5652.
- (23) Dunning, T. H. Gaussian-Basis Sets for Use in Correlated Molecular Calculations .1. The Atoms Boron through Neon and Hydrogen. *J. Chem. Phys.* **1989**, *90*, 1007-1023.
- (24) Glendening, E. D.; Reed, A. E.; Carpenter; J.E. and Weinhold, F. *NBO Version 3.1.*, Gaussian Inc., Pittsburgh. : 2003.
- (25) Frisch, M. J.; Trucks, G. W.; Schlegel, H. B.; Scuseria, G. E.; Robb, M. A.; Cheeseman, J. R.; Scalmani, G.; Barone, V.; Petersson, G. A.; Nakatsuji, H. et al. *Gaussian 16 Rev. C.01*, Wallingford, CT, 2016.
- (26) Gerardi, H. K.; DeBlase, A. F.; Su, X. G.; Jordan, K. D.; McCoy, A. B.; Johnson, M. A. Unraveling the Anomalous Solvatochromic Response of the Formate Ion Vibrational Spectrum: An Infrared, Ar-Tagging Study of the HCO₂-, DCO₂-, and HCO₂-·H₂O Ions. *J. Phys. Chem. Lett.* **2011**, *2*, 2437-2441.
- (27) Dodson, L. G.; Thompson, M. C.; Weber, J. M. Characterization of Intermediate Oxidation States in CO₂ Activation. *Annu. Rev. Phys. Chem.* **2018**, *69*, 231-252.
- (28) DePalma, J. W.; Kelleher, P. J.; Tavares, L. C.; Johnson, M. A. Coordination-Dependent Spectroscopic Signatures of Divalent Metal Ion Binding to Carboxylate Head Groups: H₂- and He-Tagged Vibrational Spectra of M²⁺·RCO₂⁻ (M = Mg and Ca, R = -CD₃, -CD₂CD₃) Complexes. *J. Phys. Chem. Lett.* **2017**, *8*, 484-488.

TOC Figure

